LANGMUIR Article
Cite This: Langmuir 2018, 34, 7284−7293
pubs.acs.org/Langmuir

Droplet Conductivity Strongly Influences Bump and Crater Formation on Electrodes during Charge Transfer

Eric S. Elton, Yash V. Tibrewala, and William D. Ristenpart*

Department of Chemical Engineering, University of California at Davis, Davis, California 95616, United States

Supporting Information

ABSTRACT: Aqueous droplets acquire charge when they contact electrodes in high voltage electric fields, but the exact mechanism of charge transfer is not understood. Recent work by Elton et al. revealed that electrodes are physically pitted during charge transfer with aqueous droplets. The pits are believed to result when a dielectric breakdown arc occurs as a droplet approaches the electrode and the associated high current density transiently locally melts the electrode, leaving distinct crater-like deformations on the electrode surface. Here we show that the droplet conductivity strongly modulates the pitting morphology but has little effect on the amount of charge transferred. Electron and atomic force microscopy shows that deionized water droplets yield no observable deformations, but as the salt concentration in the droplet increases above 10^{-3} M, the deformations become increasingly large. The observed intensity of the flash of light released during the dielectric breakdown arc also increases with droplet conductivity. Surprisingly, despite the large difference in pitting morphology and corresponding arc intensity, droplets of any conductivity acquire similar amounts of charge. These results suggest that the energy transferred during dielectric breakdown is primarily responsible for electrode pitting rather than the total amount of energy released during charge transfer.

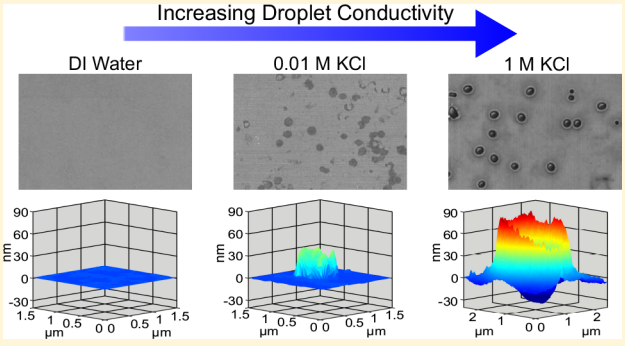

INTRODUCTION

A variety of applications involve the control of charged water droplets in electric fields. Industrially, electrocoalescence is used to enhance the phase separation of water in oil. Coulombic forces between oppositely charged water droplets induce coalescence, and the larger droplets sediment more rapidly.[1] The control of charged droplets is also of interest in microfluidic devices,[2−7] where droplet coalescence[8,9] or movement[10−13] can be controlled through application of electric fields. For example, application of an electric field can lead to droplets coalescing at a T-junction where droplets would otherwise not coalesce.[14] In addition, electric fields are used in a variety of other applications in microfluidic devices including droplet formation,[5,6] surface dewetting,[15] sorting and electroporation of cells,[16,17] solute delivery,[18] increasing mixing,[19,20] and simulation of emulsion electric properties.[21]

Although there are multiple applications involving charged droplets, it remains unclear how exactly droplets acquire charge when they contact an electrode. Previous workers have hypothesized that electrochemical reactions involving water and the electrode metal were responsible for the net charge acquired by the droplet,[4,17,22] but to date no evidence has been presented of electrochemical changes to either the droplet or electrode surface consistent with this mechanism. Recently, Elton et al. observed that electrodes were physically pitted during charge transfer with aqueous droplets.[23] The crater-shaped deformations formed during the charging of relatively high conductivity (pH 7 buffer) aqueous droplets and were approximately 0.5 μm in diameter and up to 50 nm deep. Importantly, a flash of light was observed to be emitted as a droplet approached the electrode.[23] The flash of light was interpreted in the context of dielectric breakdown (arcing) occurring when the droplet moved sufficiently close to the electrode. Since the droplet and electrode are oppositely charged prior to contact, the electric field increases dramatically as the droplet−electrode gap distance decreases.[24] Once the electric field in the gap exceeds the breakdown strength of the insulating oil, the breakdown event occurs. The formation of the observed electrode deformations was attributed to a two-step process where the electrode material first melted via Joule heating due to the high current densities present during the breakdown event. Expansion of the plasma jet of the breakdown arc then pushed the molten material radially outward where it then cooled and solidified to form craters.

A scaling analysis[23] indicated that the crater diameter scaled with the cube root of the charge transferred to the droplet (i.e., $d \sim Q^{1/3}$). However, subsequent work revealed that charge transfer to deionized water droplets did not produce similar craters, despite the droplets acquiring similar amounts of charge.[25] Instead, the electrodes appeared unchanged by the

Received: April 13, 2018
Revised: May 30, 2018
Published: June 1, 2018

Downloaded via UNIV OF CALIFORNIA DAVIS on July 4, 2018 at 17:27:14 (UTC).
See https://pubs.acs.org/sharingguidelines for options on how to legitimately share published articles.

© 2018 American Chemical Society

DOI: 10.1021/acs.langmuir.8b01234
Langmuir 2018, 34, 7284−7293

charging process. It presently remains unclear why craters formed during charge transfer to pH 7 buffer droplets but not deionized water droplets.

In this work, we systematically vary the droplet conductivity and report on changes in crater and bump formation on electrodes during charge transfer and corresponding changes in dielectric breakdown intensity. Scanning electron microscopy (SEM) and atomic force microscopy (AFM) measurements show that different conductivity droplets produce a variety of electrode pitting morphologies. Both the magnitude of the electrode deformation and dielectric breakdown intensity increase as the droplet conductivity is increased. Despite the large change in deformation morphology and corresponding change in dielectric breakdown intensity, however, aqueous droplets of all conductivities acquired similar amounts of charge. We interpret the observed changes in electrode deformation morphology in the context of an increase in heat released during the dielectric breakdown event as droplet conductivity is increased. Finally, we use these observations to provide insight into the fundamental charge transfer mechanism and offer some practical applications for devices and future investigations.

EXPERIMENTAL METHODS

The experimental setup was similar to that used in previous investigations.[23,25] Thin gold film electrodes 1 mm wide, 20 mm long, and 50 nm thick were deposited on glass substrates using standard photolithographic techniques. For each experiment, two new electrodes were placed in a plastic cuvette with nonconductive spacers at the top and bottom and filled with 100 cSt silicone oil. One electrode was connected to a high voltage supply (Trek 610E). The other was grounded through an electrometer (Keithley 6514) used to measure the current flowing through the system (Figure 1, top). After

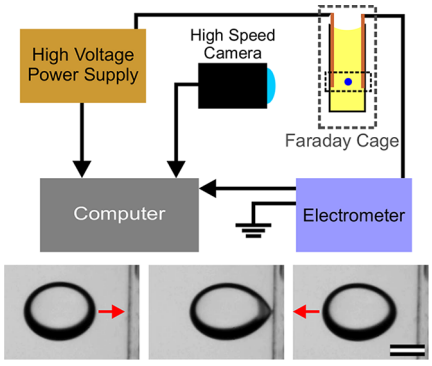

Figure 1. Top: schematic of experimental setup (not to scale). Bottom: representative images from a high-speed video of a 3.5 μL 0.1 M KCl droplet approaching, making apparent contact with and departing from an electrode. The red arrows indicate the direction of droplet motion. Scale bar is 1 mm. See also the movie in the Supporting Information.

the electrical connections were made to the cuvette, but prior to droplet insertion, a Zerostat 3 antistatic gun was used to remove static charge on the exterior of the cuvette.

After the high voltage was applied, a 3.5 μL droplet was pipetted between the electrodes using a micropipet. The droplet is initially drawn toward one of the electrodes where it makes contact, becomes charged, and is repelled toward the opposite electrode where the process repeats (see Supporting Information movie). The density difference between the oil and droplet caused the droplet to slowly settle toward the bottom of the cuvette. When the droplet was close to the end of the electrodes, positive dielectrophoretic forces kept the droplet from moving any lower,[26] and the droplet bounced in approximately the same location for the remainder of the experiment. A high-speed camera (Phantom v7.3) was used to visually observe the droplet with a frame rate of 500 frames/s, while the analogue signal from the electrometer was recorded using a data acquisition card at a sampling frequency of 50 kHz. Droplets were typically allowed to bounce for 30 min, representing thousands of charge transfer events. At the end of each experiment, the droplet was removed with a pipet and the electrodes were washed with hexane, acetone, and water to remove the silicone oil.

Figure 1, bottom, shows representative still images from a high-speed video of a 3.5 μL 0.1 M KCl droplet approaching, contacting, and departing from an electrode. The droplet deforms to form a pointed tip known as a Taylor cone as it approaches the electrode.[27] This important characteristic of droplet deformation behavior that has been widely reported previously;[4,9,10,12,17,18,22,23,25,28] however, charge transfer can occur between electrodes and conducting particles of other shapes.[19,23,24,29−31] The main goal here is to investigate the role of droplet conductivity on charge transfer and electrode deformation during charge transfer events.

We observed the electrical bouncing of aqueous droplets with a range of conductivity between 0.001 and 113 mS/cm. Droplet conductivity was controlled through the addition of potassium chloride (KCl) in varying concentrations to deionized water. The conductivity of the bulk solution was measured immediately prior to each experiment.

The charge on the droplet was determined using a standard force balance technique.[18,25,28] In brief, during periods of constant velocity, the electrostatic force ($F_E = QE$) is balanced with the drag force ($F_D = 4\lambda\pi\mu aU$). The resulting droplet charge is given as $Q = \frac{4\pi\mu aU}{E}$, where μ is the oil viscosity, a the droplet radius, U the droplet velocity, and E the applied electric field. The Hadamard−Rybczynski correction factor λ is 1 since the viscosity of the water droplet is much less than that of the surrounding silicone oil.[32,33] The electric field is approximated as $E = V/H$, where V is the applied voltage and H is the distance between the electrodes. For all experiments outlined here, the applied voltage was 3.3 kV, yielding a nominal electric field of 4.1 kV/cm. The droplet velocity was determined using standard image analysis algorithms to detect the change in centroid position of the drop between each frame of the recorded high-speed video.

A photomultiplier tube (PMT) was also used to quantify the light intensity of the dielectric breakdown event as the droplet approached the electrode. During these experiments, it was not possible to simultaneously visually observe the droplet and measure the breakdown light intensity, so the droplet charge could not be estimated using the above force balance technique. Instead, we performed a nonlinear regression of a model of the system current to the observed current to extract the droplet charge using a methodology described elsewhere.[25] This technique does not depend on visual observation of the droplet, although the droplet radius was estimated via the ostensible droplet volume.

Electrodes were washed with hexane, acetone, and water to remove the silicone oil after each experiment. Scanning electron microscopy (SEM) images of the electrode surfaces were taken using an FEI Scios DualBeam SEM with a 5 kV accelerating voltage. Atomic force microscopy (AFM) images were using at Veeco Multimode AFM in tapping mode.

RESULTS

Examination of all electrodes after experimentation did not reveal any changes visible to the naked eye. Under optical microscopy examination, however, subtle visible changes were observed on the positive electrodes on which high conductivity droplets (0.1 and 1 M KCl, 11.8 and 113 mS/cm) were allowed to charge (Figure S1), which is similar to previous reports.[23] No other electrodes exhibited changes visible via standard optical microscopy.

DOI: 10.1021/acs.langmuir.8b01234
Langmuir 2018, 34, 7284−7293

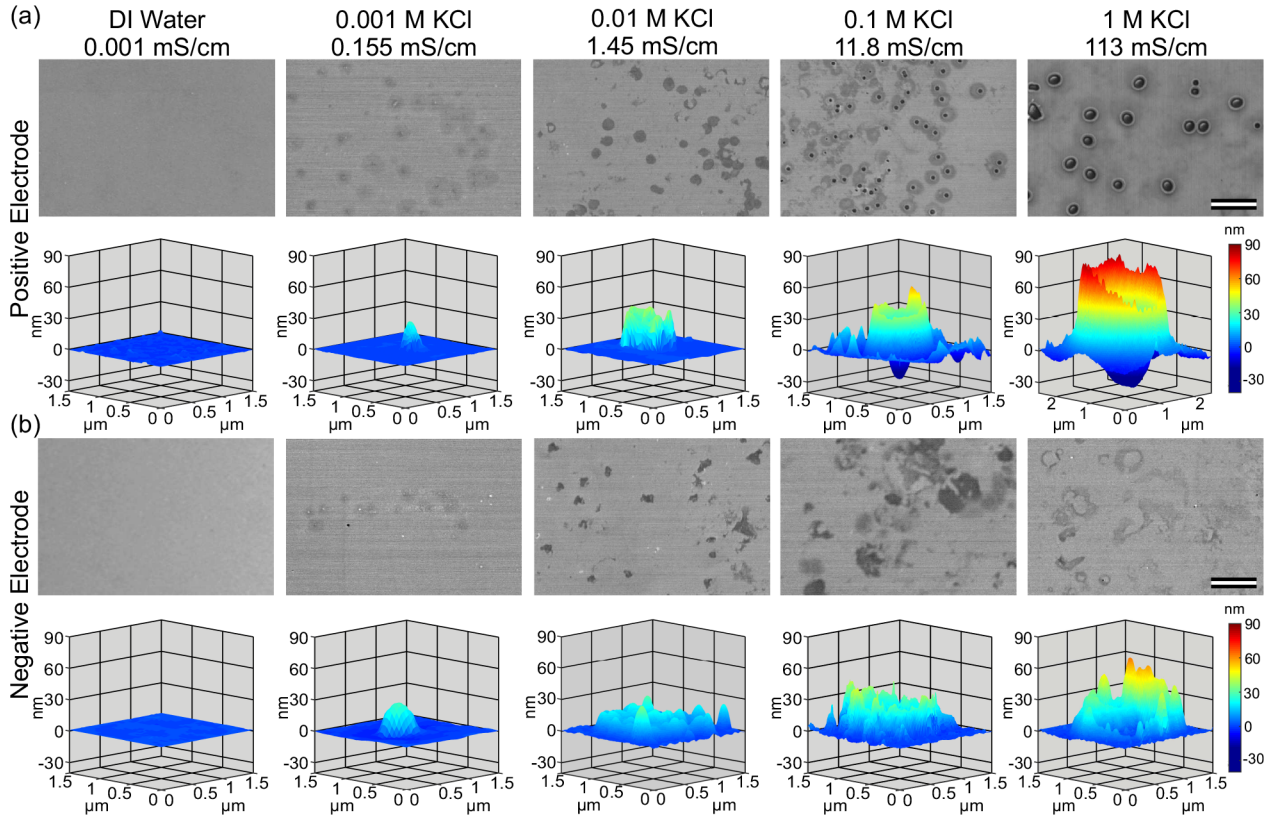

Figure 2. Deformation morphology versus droplet conductivity. SEM images (top row) and AFM images (second row) of deformations formed on positive electrodes (a) and negative electrodes (b) during the charging of aqueous droplets of various KCl concentrations. SEM images show many deformations while AFM images show only a single deformation. Droplet KCl concentration and measured conductivity are displayed above each column. Scale bar is 5 μm for all images.

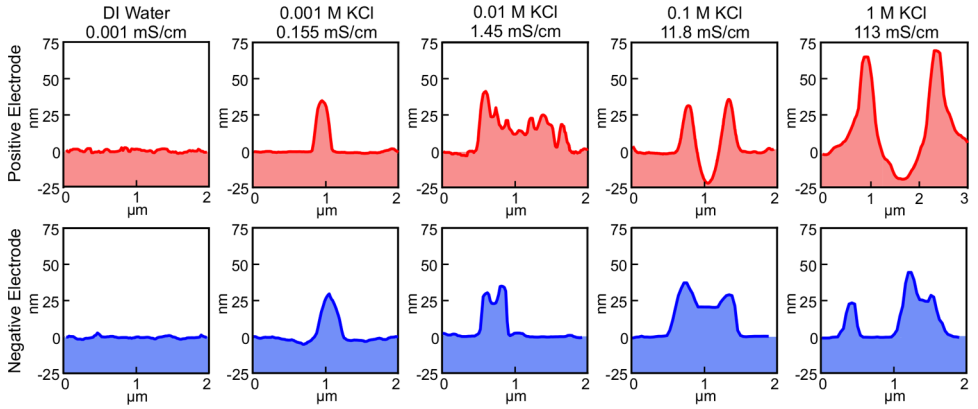

Figure 3. Representative height profiles of deformations formed on positive (top row) and negative (bottom row) electrodes. Profiles were extracted from AFM images of individual deformations. Deformations are only observed to form below the surface of the electrode on positive electrodes with 0.1 and 1 M KCl droplets. No deformations were observed for form on the surface of electrodes during the charging of deionized water droplets. Droplet KCl concentration and measured conductivity are displayed above each column.

Higher magnification scanning electron microscope (SEM) images of the electrode surfaces reveal changes to the electrodes (Figure 2), with the type of change dependent on the droplet conductivity. On both positive and negative electrodes, there are no apparent changes to the surface of the electrode after low conductivity (0.001 mS/cm) deionized water droplets were allowed to charge. Faint darker areas are present on the positive electrodes on which intermediate conductivity (0.001 and 0.01 M KCl, 0.155 and 1.45 mS/cm) were bounced. The radius of the dark regions is approximately the same (0.65 μm) for all droplet conductivities (Figure S2), although the regions become darker and more pronounced as the droplet conductivity increases. Finally, craters (as opposed to the "bumps" observed at lower conductivities) were observed on the positive electrodes on which high conductivity (0.1 and 1 M KCl, 11.8 and 113 mS/cm) droplets were bounced. The craters are larger for higher conductivity droplets. We emphasize that the intermediate conductivity droplets did not yield the deep craters observed from the charging of higher conductivity droplets.

A similar trend is also observed on the negative electrode, albeit without any crater formation under the conditions tested

DOI: 10.1021/acs.langmuir.8b01234
Langmuir 2018, 34, 7284−7293

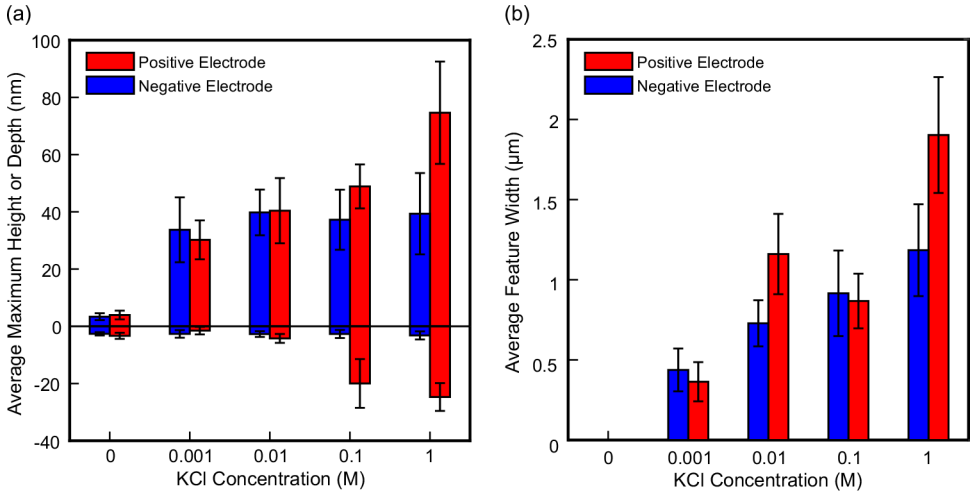

Figure 4. Deformation dimensions vary with droplet conductivity. (a) Average deformation height and depth observed from AFM images of individual deformations created on positive (red) and negative (blue) electrodes during the charging of aqueous droplets of various KCl concentrations. The height and depth reported for deionized water droplets (0 M KCl) represent typical variation in electrode surfaces as measured using AFM. Error bars represent one standard deviation from the mean. (b) Average deformation diameter on positive (red) and negative (blue) electrodes as determined from image analysis of AFM images of individual deformations. No deformations were observed to form during the charging of deionized water droplets. Error bars represent one standard deviation from the mean.

here (Figure 2b). While there are no apparent changes to the negative electrode on which deionized water droplets were bounced, faint dark areas appear on electrodes on which intermediate conductivity droplets were bounced. Again, the dark areas become more pronounced as the droplet conductivity increased. Large and apparently overlapping features appear on the negative electrodes on which high conductivity droplets were bounced.

Importantly, for all electrodes, the observed changes were only present in a relatively small area of the electrode, presumably in the immediate vicinity of where the droplet had been bouncing. The electrode surface outside of this area appeared unchanged. Control experiments in which electrodes were placed in an oil filled cuvette with an applied voltage, but no droplet revealed no changes to the electrode surface. Finally, examination of the chemical composition of the electrode surface using energy dispersive spectroscopy (EDS) did not show any discernible chemical changes to the surface of the electrode, despite the apparent physical changes.

The morphology of the bumps and craters was determined using tapping mode atomic force microscopy (AFM) (cf. Figures 2 and 3). The AFM images confirm that there are no changes to the surface of electrodes on which deionized water droplets were allowed to charge; the AFM images of these electrodes are similar to those of unused electrodes. As the droplet conductivity is increased, small bumps (0.001 M KCl) and then uneven bumps (0.01 M KCl) began to form on the surface of both positive and negative electrodes. Craters are observed to form on positive electrodes as the result of charge transfer with 0.1 and 1 M KCl droplets. In contrast, no craters were observed to form on the surface of the negative electrode. Instead, uneven bumps were observed to form as a result of the charging of KCl droplets on negative electrodes.

Figure 4 shows the average maximum height, depth, and width of the deformations formed on positive and negative electrodes by the charging of different conductivity droplets. In general, the maximum height of the craters and bumps on positive electrodes increases as the conductivity of the bounced droplet increases (Figure 4a). On negative electrodes, the bumps consistently rise to around 40 nm above the surface of the electrode regardless of the conductivity of the droplet. The small bars in Figure 4a for deionized water droplets (0 M KCl) represent the typical 3−4 nm variations in height found on the surface of all electrodes. Similar variations were found on recently fabricated (unused) electrodes. The average crater or bump diameter, found using standard image analysis algorithms to identify the enclosed area of the region that rose above the surface of the electrode, increases from less than 0.5 μm to as high as 2.4 μm on both positive and negative electrodes as the conductivity of the droplet increased (Figure 4b).

Measurements of the droplet charge from analysis of the recorded high-speed video of droplet transit indicate that despite the 5 orders of magnitude difference in droplet conductivity, all droplets acquired similar amounts of charge (Figure 5). Each marker in Figure 5 represents an individual experiment (unique droplet and electrodes), with each experiment consisting of approximately 200 individual charge transfer events. There is significant trial-to-trial variability in these measurement, which may be due to changes in the electric field from small changes in the exact electrode placement or from static charge on the surface of the cuvette.[34] The trial-to-trial variation in charges measured at one concentration are larger than any systematic difference across all concentrations. There is no apparent correlation between droplet conductivity and the amount of charge transferred to droplets.

Our previous report of crater formation on electrodes during charge transfer with aqueous droplets revealed flashes of light consistent with dielectric breakdown as the droplet approached the electrode.[23] Here, we also observed evidence of dielectric breakdown occurring as droplets approached the electrode, as indicated by similar flashes of light detected by a photomultiplier tube (PMT) focused on the droplet/electrode interface as the droplet approached the electrode. Peaks in the PMT current indicating a release of light were observed simultaneously with peaks in the current flowing through the electrometer (i.e., the "system current") when the droplet was in view of the PMT (Figure 6a,b). A crucial observation is that

DOI: 10.1021/acs.langmuir.8b01234
Langmuir 2018, 34, 7284−7293

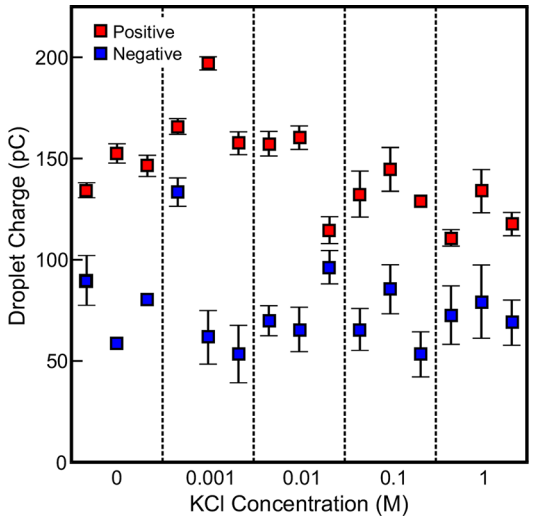

Figure 5. Average positive (red) and negative (blue) charge acquired by 3.5 μL aqueous droplets of different KCl concentrations bouncing between electrodes in a 0.4 kV/mm electric field. Experiments were carried out in triplicate for each drop KCl concentration with unique electrodes being used for each experiment. Each marker represents a single experimental trial of approximately 200 charge transfer events. Error bars represent one standard deviation from the mean.

the average intensity of the light released as the droplet approached the electrode increased as the droplet conductivity increased (Figure 6c). Qualitatively similar flashes of light consistent with dielectric breakdown were observed at both positive and negative electrodes regardless of electrode power (at both grounded and high voltage electrodes). No evidence of dielectric breakdown (i.e., no flashes of light) was ever observed as deionized water droplets approached electrodes.

Even at higher conductivities, a flash of light was not observed during every charge transfer event. Figure 6d shows the percentage of charge transfer events during which a flash of light was detected. In general, the percentage of charge transfer events that produced flashes of light increased with droplet conductivity. It is unclear why some charge transfer events produced flashes of light while others did not. Regardless of whether or not a flash of light was emitted, the droplet underwent charge transfer and moved away from the electrode afterward.

The maximum system current that was recorded as the droplet contacted the electrode increased slightly as droplet conductivity was increased (Figure 6e). It is unclear if this increase is related to the increase in current during the dielectric breakdown event or not; the increase is not always observed when many trial replicates using different sets of electrodes are used (Figure S3b). We also did not observe any

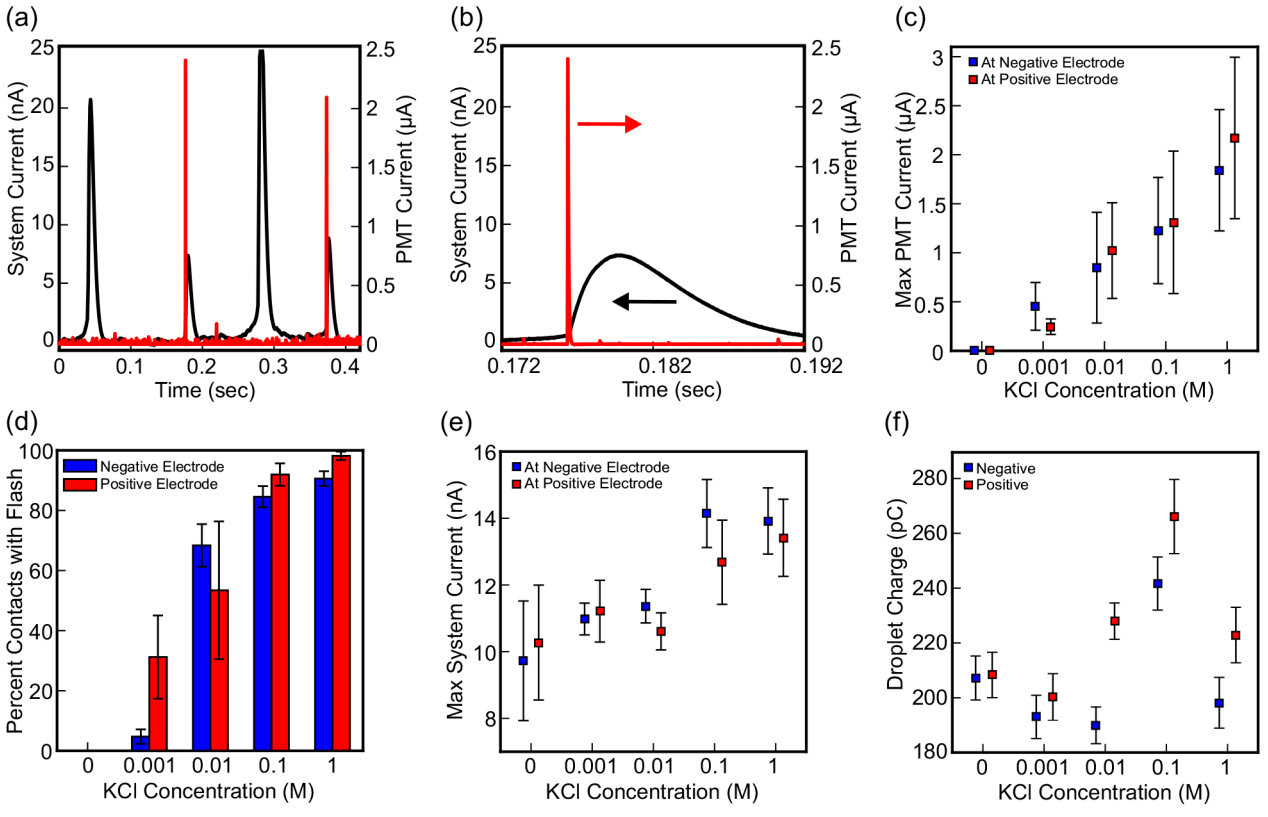

Figure 6. Evidence of dielectric breakdown during charge transfer. (a) Representative system current (black) and photomultiplier tube (PMT) current (red) recorded simultaneously as a 3.5 μL 1 M KCl droplet bounced between electrodes. Simultaneous peaks in the PMT current and system current occur when the droplet approaches the electrode in view of the PMT. (b) Magnified view of the first peak in (a). (c) Average maximum PMT current recorded as droplets approached electrodes. No flashes of light were observed during the charging of deionized water droplets (0 M KCl). Each data point is the average of at least 200 data points. (d) Average percentage of charge transfer events during which a flash of light was observed as droplets of different KCl concentrations approached electrodes. Each bar represents the average of at least six individual trials of approximately 90 bounces each. (e) Average maximum recorded system current and (f) average charge acquired by droplets of different KCl concentrations acquired during contact with the electrode in view of the PMT. For all plots, error bars represent one standard deviation from the mean. Data acquired at the positive electrode are red while data from the negative electrode are blue.

DOI: 10.1021/acs.langmuir.8b01234
Langmuir 2018, 34, 7284−7293

noticeable differences in the current peak width at half-height as the droplet conductivity was increased (Figure S3c). Importantly, the droplet charge did not increase as the droplet conductivity increased (Figure 6f), and is thus not correlated to dielectric breakdown intensity.

The results shown in Figures 2−6 were all obtained using gold electrodes. To test whether craters are observed to form on positive electrodes of other metals, we also fabricated tungsten thin film electrodes. Tungsten was chosen because it has an extremely high melting point temperature. When 0.1 M KCl droplets are bounced between tungsten electrodes, bumps are observed to form on the positive electrode (Figure 7). The

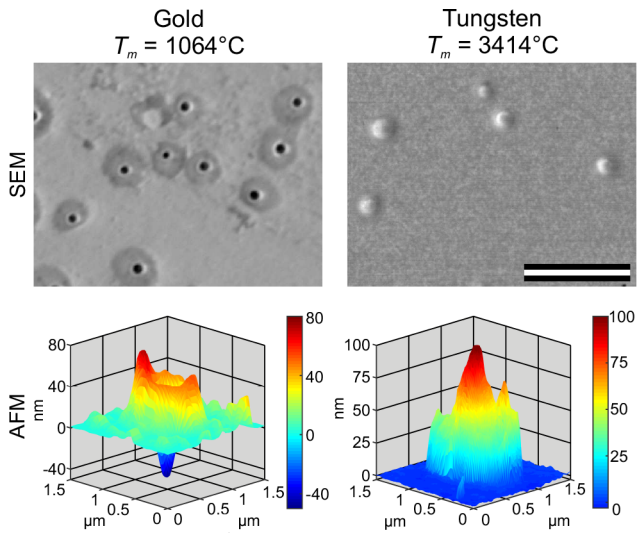

Figure 7. SEM (top) and AFM (bottom) images of craters and bumps formed on the surface of gold (left) and tungsten (right) electrodes by the charging of a 0.1 M KCl droplet. SEM images show multiple deformations while AFM images show one single deformation. Scale bar is 5 μm for both images.

bumps rise approximately 80−100 nm above the surface of the electrode and are similar in diameter to the craters observed to form on positive gold electrodes. Similar features to those observed on negative gold electrodes are observed to form on negative tungsten electrodes.

DISCUSSION

Previous work by Elton et al. suggested that crater formation is a two-step process.[23] First, the electrode melts due to Joule heating from high current densities present during charge transfer. Second, expansion of the plasma jet present in the dielectric breakdown event pushes the molten material outward where it solidifies to form the crater. Dielectric breakdown is key to the mechanism to provide both the high current density necessary to melt the electrode as well as the radial momentum to move the molten material outward.

The results presented here indicate that a variety of morphologies can be formed on the surface of electrodes by the charging of different conductivity droplets. Intermediate conductivity droplets formed bumps on the surface of both positive and negative electrodes during charge transfer. High conductivity droplets also produced bumps on negative electrodes but, in contrast to all other droplets, produced craters on positive electrodes.

It is apparent that the intensity of the dielectric breakdown, as evidenced by light emission, is highly correlated to the formation of bumps and craters on the surface of the electrode. High intensity breakdowns are correlated to crater formation, suggesting that lower intensity breakdowns provide enough energy to deform the electrode, but not to melt it and form craters. This hypothesis is supported by the formation of bumps on the surface of positive tungsten electrodes when 0.1 M KCl droplets were bounced on them (cf. Figure 7). Tungsten has a higher melting temperature than gold. Assuming that similar amounts of energy are dissipated into the electrode during charge transfer, the gold electrode will melt but the tungsten electrode will not. The observation of bumps forming on tungsten electrodes under conditions where craters form on gold electrodes suggests that the electrode material first bulges before melting and forming a crater.

What causes the electrode material to bulge prior to crater formation? Qualitatively similar bumps and craters are observed to form on thin gold films on glass substrates when irradiated with nanosecond laser pulses.[35−38] At pulse energies below the ablation level, small hollow bumps are observed to form on the film surface. As the laser pulse energy is increased, the bumps become wider and taller. At sufficiently high pulse energies, craters qualitatively similar those observed here form.[35,36] The bumps and craters form from the thermal expansion of the solid film pushing the center of the heated area upward and the thermoplastic deformation of the heated film, leading to the observed permanent deformations.[39−42]

We hypothesize that a similar process creates the bumps formed during charge transfer with aqueous droplets. The solid metal electrode film is rapidly heated leading to rapid thermal expansion which causes the middle of the heated region to move upward and rise off the substrate surface. The elevated temperature of the film allows for it to plastically deform and remain raised even after cooling.

Estimates of the thermal expansion distance of the solid metal film suggest that a large enough area of the electrode is heated for the film to expand to the final observed shape. For the smallest bumps observed, a total expansion of 4 nm is needed to push the film to the observed dimensions (see Supporting Information for details). The total temperature change ΔT needed to produce an expansion of 4 nm can be found by[43]

$$\Delta T = \frac{\Delta R}{\alpha R} \tag{1}$$

Here R is the total heated radius, ΔR is the total thermal expansion distance (4 nm), and α is the thermal expansion coefficient of the material. While we cannot directly observe the width of the plasma beam in our experiments, we estimate R by measuring the radius of the dark region surrounding each crater and bump in the SEM images (cf. Figure 2). We believe this is a reasonable estimate of the plasma diameter since these features are observed on all electrodes on which dielectric breakdown was observed during charge transfer. The average radius of this roughly circular region was 0.65 μm for all electrodes on which droplets between 0.001 and 0.1 M KCl were bounced (Figure S2). The dark region may result from changes in the grain structure of the film during heating or possibly the deposition of a thin layer of polymerized silicone oil onto the electrode surface during charge transfer. Similar dark regions were previously observed to form as a result of charge transfer to metal particles.[23]

DOI: 10.1021/acs.langmuir.8b01234
Langmuir 2018, 34, 7284−7293

Substitution of appropriate values into eq 1 indicates that on gold electrodes a circular region with a radius of 0.65 μm would need to be heated to 465 °C to expand the 4 nm necessary to produce the observed bumps, a temperature well below the melting point of gold. To produce similar sized bumps on tungsten electrodes the electrode would need to be heated to 1393 °C, which is below the melting point of tungsten but higher than the melting point of gold. This result is consistent with the notion that similar amounts of energy will lead to film expansion and bump formation on tungsten electrodes while melting and forming craters on gold electrodes.

A scaling analysis of the amount of energy released during charge transfer suggests that enough energy is present to raise the electrode to the needed temperatures. The amount of energy released due to Joule heating is found by integrating the power over the time period of charge transfer and can be estimated as $H \approx Pt \approx VIt \approx VQ$, where V is the voltage difference between the droplet and electrode, I is the current flowing between the droplet and electrode, t is the time period over which current flows, and $Q = It$ is the charge acquired by the droplet. We can estimate the surface potential of the droplet by treating it as a conducting sphere containing the measured charge (see Supporting Information for more details). For a droplet carrying 100 pC of charge, the surface voltage will be approximately 500 V, and $H \approx 50$ nJ. By comparison, the heat needed to raise a volume of tungsten 0.65 μm in radius and 50 nm thick to 1393 °C is approximately 0.25 nJ, or 0.5% of the amount of energy released during charge transfer. Even less energy (0.08 nJ) is needed to raise the same volume of gold to 465 °C. This conservative scaling estimate suggests that only a fraction of the charge acquired by the droplet must be transferred via dielectric breakdown to heat the electrode to the temperature needed for deformation.

This analysis neglects more complicated heating effects including uneven heating in the plasma beam and heat diffusion into the rest of the electrode film. It also assumes that the film will expand similarly to bulk metal. Nonetheless, it suggests that heating of the film via dielectric breakdown provides the thermal expansion necessary to form the observed bumps.

The observed bumps and craters are believed to form during the transient heating of the electrode via energy delivered by the plasma during the dielectric breakdown event. During the charging of low conductivity droplets, no dielectric breakdown is observed, and no deformations are observed to form on the surface of the electrode (Figure 8, top). When intermediate conductivity droplets approach electrodes, weak dielectric breakdown occurs, and the electrode film thermally expands and forces the center to rise into the observed smooth bumps. As the droplet conductivity is increased, the breakdown energy increases, and the bumps become irregularly shaped (Figure 8, middle). This may be caused by the partial melting of the metal film as it expands. Variations in size, density, and temperature of the plasma and heated silicone oil interacting with the molten electrode could cause complex hydrodynamic effects, resulting in the observed roughness. At sufficiently high breakdown energies, such as those observed during the charging of high conductivity droplets, the electrode film melts completely and is pushed outward by the plasma to form the observed craters (Figure 8, bottom).

It is clear that despite similar dielectric breakdown intensities at both positive and negative electrodes (cf. Figure 6c), craters are only formed by the charging of high conductivity droplets on positive electrodes while the same droplets form bumps on

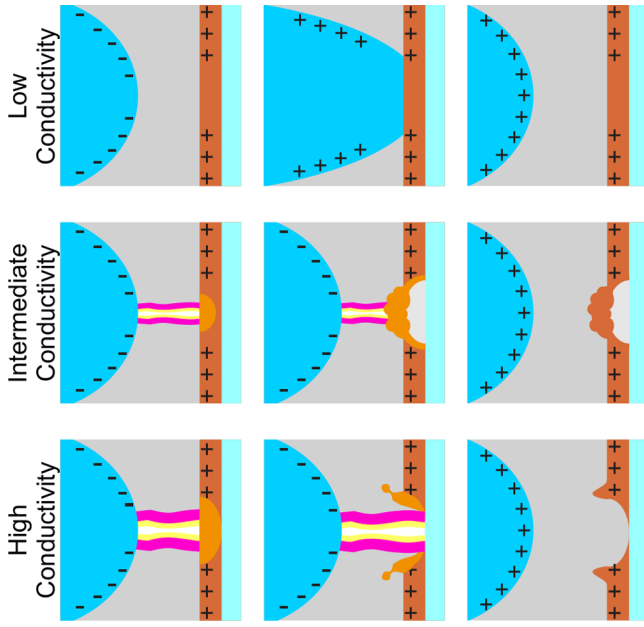

Figure 8. Schematic of electrode deformation mechanism during charge transfer with low, intermediate, and high conductivity droplets.

negative electrodes. This is true regardless of the polarity of the powered electrode. While it is unclear why the polarity of the electrode affects the shape of the observed bump or crater, it is known that breakdown events move preferentially from positive to negative surfaces,[44,45] so the positive electrode may have more time to heat, melt, and proceed to crater formation during the charge transfer event than the negative electrode. The exact process of dielectric breakdown in oils is not well understood,[45] so more complex phenomena may also be occurring.

Previous work estimated the crater diameter from the solution to the transient heat equation with a point heat source.[23] These estimates indicated that the crater diameter scaled with the amount of charge transferred to the droplet to the 1/3 power. It was assumed that the entire charge acquired by the droplet was transferred through the dielectric breakdown event. The results presented here indicate that while dielectric breakdown is necessary for electrode deformation, only the energy released during the dielectric breakdown leads to electrode deformation, not the entire energy released during charge transfer. This is consistent with the observation that droplets of all conductivities acquire similar amounts of charge regardless of the intensity of the dielectric breakdown or electrode deformation morphology. It is difficult to estimate the amount of energy released during the dielectric breakdown since there are no noticeable differences in the recorded current as the droplet conductivity is varied (cf. Figure S3). Previous estimates of crater diameter included a fitting factor of 0.2,[23] consistent with the notion that using the entire energy released during charge transfer provided an overestimate of the energy needed for crater formation.

Finally, what causes the increase in dielectric breakdown intensity as the droplet conductivity is increased? Our experiments rule out the simple explanation that lower conductivity droplets acquire less charge, which would lead to a lower electric field strength between the droplet and electrode. Measurements of the droplet charge instead indicate that despite the 5 orders of magnitude change in conductivity, all droplets obtained similar amounts of charge (Figure 5). This

DOI: 10.1021/acs.langmuir.8b01234
Langmuir 2018, 34, 7284−7293

result seemingly differs from previous work that indicated higher conductivity droplets acquired less charge than lower conductivity droplets, although the effect of droplet conductivity was diminished for larger droplets in higher electric fields.[18] In our experiments, we use a much larger droplet than the previous work (3.5 vs 1 μL) and a high electric field (4.1 vs 4.4 kV/cm). Thus, the lack of difference in charge acquired by different conductivity droplets observed here is broadly consistent with this previous report.

Droplets were also observed to always acquire more positive charge than negative charge. This is consistent with multiple previous observations (see ref 25 for a review of these reports). Recent work by Yang et al. suggests that the difference in charge acquired may be due to uneven electric fields caused by static charge on the plastic cuvette holding the electrodes since, when the cuvette surface was wiped with isopropanol to remove static charge, the observed charge disparity decreased.[34] We used a similar experimental apparatus as Yang et al. but made no attempt to measure or control any residual static charge on the cuvette. On average, we observed a charge disparity of approximately 200%, which is larger than the 25% difference observed by Yang. It is unclear what is causing this charge disparity, although residual static charge on the cuvette or the glass substrate may be contributing. More work is needed to fully understand all causes of this charge disparity.

Another possibility for the increase in dielectric breakdown intensity as droplet conductivity increases is that the droplet conductivity directly affects the ability of the droplet to provide enough charge carriers rapidly enough to enable dielectric breakdown. Similar increases in light intensity were observed during dielectric breakdown between stationary solid electrodes and charged aqueous solutions (i.e., more conductive solutions produced brighter arcs than lower conductivity solutions).[46−48] This behavior was attributed to changes in the charge relaxation time of the liquid given by $t_c = \epsilon\epsilon_0/\sigma$, where σ and $\epsilon\epsilon_0$ are the liquid conductivity and permittivity. As the liquid conductivity increases, the charge relaxation time decreases, and charges are able to move faster and sustain a more intense dielectric breakdown event.[46]

The qualitative similarity of the intensity of breakdown events between stationary electrodes investigated previously and the moving droplet and stationary electrode system studied here suggests that a similar mechanism is operative. The observed flashes of light occur over approximately 15 μs or less, suggesting that the charge relaxation time needs to be as fast or faster for the droplets to provide enough charge to sustain breakdown. In our experiments, the charge relaxation time varies from 10^{-5} to 10^{-10} s as the droplet conductivity is increased. This range of charge relaxation times suggests that low conductivity droplets cannot provide enough charge carriers to sustain dielectric breakdown in the microseconds before the droplet contacts the electrode.

The effect of droplet permittivity was not explored in our experiments, although lower permittivity droplets are expected to have smaller dielectric breakdown intensities based on the charge relaxation time. The droplet permittivity may also influence the amount of charge the droplet acquires since the charge relaxation time may limit the amount of charge the droplet can acquire while in contact with the electrode.

CONCLUSION

We examined the effect of droplet conductivity on the formation of bumps and craters on electrodes during charge transfer. As the droplet conductivity increased, the observed bumps became larger until, at sufficiently high conductivities, craters were formed. No features were observed on electrodes as the result of the charging of deionized water droplets. The intensity of the dielectric breakdown which occurred as droplets approach electrodes increased as the droplet conductivity increased. At low breakdown energies, the electrode film is not melted completely, and thermal expansion of the solid film causes it to bulge upward, forming the observed bumps. When the breakdown energy is sufficient to melt the electrode film completely, the plasma jet pushes the molten material outward to form craters.

The observations presented here offer insight into the basic mechanism of charge transfer between electrodes and liquid droplets. Although dielectric breakdown occurs between electrodes and KCl droplets, breakdown is not needed for droplet charging as evidenced by the charging of deionized water droplets without any evidence of dielectric breakdown. Furthermore, droplets acquire similar amounts of charge regardless of the presence or intensity of dielectric breakdown. This result suggests that some other process occurs during droplet contact with the electrode to transfer charge. One possibility is that electrochemical reactions, such as the reduction and oxidation of water or of the electrode material, lead to the net charge on the droplet.[4,12,22] The current work does not elucidate what other mechanism is responsible for droplet charging. More work is needed to fully understand the complete droplet charging process.

Previous reports of light emission between two charged droplet approaching each other in air suggest that a similar mechanism for charge transfer involving dielectric breakdown is also applicable for charge transfer between two droplets.[49,50] Importantly, previous work has revealed that the amount of charge transferred between two droplets is largely independent of droplet conductivity.[9] This is consistent with the results presented here which suggest that the amount of charge the droplet acquires is not dependent on the intensity of the dielectric breakdown event. More research is needed to fully examine the role of dielectric breakdown during charge transfer between two droplets.

In terms of practical applications, the results shown here are applicable to the design of lab-on-a-chip,[4,14] electrocoalescers,[1] electrowetting,[51] inkjet printers,[52] and other devices[4,8,9] which use electric fields to control charged droplets. For sufficiently high droplet conductivities, thin electrodes may be significantly degraded after continued use. This may be particularly important for electrocoalescers which typically use salty water to increase droplet coalescence.[1,53] Importantly, it appears that the bumps observed here do not affect the bulk electrode function; that is, the entire electrode remains conductive when covered in bumps. The local electric field, however, may be disrupted which may affect the charge transfer between the electrode and other objects. The disruption of the electric field may complicate efforts to corroborate the prediction of the theoretical maximum amount of charge a droplet or particle can acquire from a planar electrode, since the electrode surface is no longer planar.[23,25,30,31] Finally, the submicrometer size and shape of the craters and bumps point to a possible mechanism to pattern thin films on length scales current not afforded by lithography and laser ablation techniques.[54]

DOI: 10.1021/acs.langmuir.8b01234
Langmuir 2018, 34, 7284−7293

■ ASSOCIATED CONTENT

Supporting Information

The Supporting Information is available free of charge on the ACS Publications website at DOI: 10.1021/acs.langmuir.8b01234.

Figures S1−S3; derivation of needed thermal expansion distance (PDF)

Video of a 3.5 μL droplet bouncing between electrodes in silicone oil (MPG)

■ AUTHOR INFORMATION

Corresponding Author

*E-mail: wdristenpart@ucdavis.edu (W.D.R.).

ORCID

William D. Ristenpart: 0000-0002-4935-6310

Notes

The authors declare no competing financial interest.

■ ACKNOWLEDGMENTS

We thank the UC Davis Center for Nano-Micro Manufacturing for use of their equipment in electrode fabrication and SEM characterization. We also acknowledge and thank Adam Moule for use of his AFM. Finally, we thank the NSF Particulate and Multiphase Processes program for support (award 1707137).

■ REFERENCES

(1) Eow, J. S.; Ghadiri, M.; Sharif, A. O.; Williams, T. J. Electrostatic enhancement of coalescence of water droplets in oil: a review of the current understanding. *Chem. Eng. J.* **2001**, *84*, 173−192.

(2) Baroud, C. N.; Gallaire, F.; Dangla, R. Dynamics of microfluidic droplets. *Lab Chip* **2010**, *10*, 2032−2045.

(3) Seemann, R.; Brinkmann, M.; Pfohl, T.; Herminghaus, S. Droplet based microfluidics. *Rep. Prog. Phys.* **2012**, *75*, 016601.

(4) Beránek, P.; Flittner, R.; Hrobař, V.; Ethgen, P.; Přibyl, M. Oscillatory motion of water droplets in kerosene above co-planar electrodes in microfluidic chips. *AIP Adv.* **2014**, *4*, 067103.

(5) Vobecká, L.; Khafizova, E.; Stragier, T.; Slouka, Z.; Přibyl, M. Electric field driven addressing of ATPS droplets in microfluidic chips. *Microfluid. Nanofluid.* **2017**, *21*, 51.

(6) Chong, Z. Z.; Tan, S. H.; Ganan-Calvo, A. M.; Tor, S. B.; Loh, N. H.; Nguyen, N.-T. Active droplet generation in microfluidics. *Lab Chip* **2016**, *16*, 35−58.

(7) Im, D. J. Next generation digital microfluidic technology: Electrophoresis of charged droplets. *Korean J. Chem. Eng.* **2015**, *32*, 1001−1008.

(8) Ristenpart, W. D.; Bird, J. C.; Belmonte, A.; Dollar, F.; Stone, H. A. Non-coalescence of oppositely charged drops. *Nature* **2009**, *461*, 377−380.

(9) Hamlin, B. S.; Creasey, J. C.; Ristenpart, W. D. Electrically tunable partial coalescence of oppositely charged drops. *Phys. Rev. Lett.* **2012**, *109*, 094501.

(10) Cartier, C. A.; Graybill, J. R.; Bishop, K. J. M. Electric generation and ratcheted transport of contact-charged drops. *Phys. Rev. E: Stat. Phys., Plasmas, Fluids, Relat. Interdiscip. Top.* **2017**, *96*, 043101.

(11) Zagnoni, M.; Le Lain, G.; Cooper, J. M. Electrocoalescence mechanisms of microdroplets using localized electric fields in microfluidic channels. *Langmuir* **2010**, *26*, 14443−14449.

(12) Im, D. J.; Yoo, B. S.; Ahn, M. M.; Moon, D.; Kang, I. S. Digital electrophoresis of charged droplets. *Anal. Chem.* **2013**, *85*, 4038−4044.

(13) Gu, H.; Murade, C. U.; Duits, M. H. G.; Mugele, F. A microfluidic platform for on-demand formation and merging of microdroplets using electric control. *Biomicrofluidics* **2011**, *5*, 011101.

(14) Link, D. R.; Grasland-Mongrain, E.; Duri, A.; Sarrazin, F.; Cheng, Z. D.; Cristobal, G.; Marquez, M.; Weitz, D. A. Electric control of droplets in microfluidic devices. *Angew. Chem., Int. Ed.* **2006**, *45*, 2556−2560.

(15) Lee, S.; Lee, S.; Hwang, H.; Hong, J.; Lee, S.; Lee, J.; Chae, Y.; Lee, T. Ultrafast single-droplet bouncing actuator with electrostatic force on superhydrophobic electrodes. *RSC Adv.* **2016**, *6*, 66729−66737.

(16) Clausell-Tormos, J.; Lieber, D.; Baret, J. C.; El-Harrak, A.; Miller, O. J.; Frenz, L.; Blouwolff, J.; Humphry, K. J.; Köster, S.; Duan, H.; Holtze, C.; Weitz, D. A.; Griffiths, A. D.; Merten, C. A. Droplet-based microfluidic platforms for the encapsulation and screening of mammalian cells and multicellular organisms. *Chem. Biol.* **2008**, *15*, 427−437.

(17) Im, D. J.; Jeong, S. N.; Yoo, B. S.; Kim, B.; Kim, D. P.; Jeong, W. J.; Kang, I. S. Digital microfluidic approach for efficient electroporation with high productivity: transgene expression of microalgae without cell wall removal. *Anal. Chem.* **2015**, *87*, 6592−6599.

(18) Im, D. J.; Noh, J.; Moon, D.; Kang, I. S. Electrophoresis of a charged droplet in a dielectric liquid for droplet actuation. *Anal. Chem.* **2011**, *83*, 5168−5174.

(19) Cartier, C. A.; Drews, A. M.; Bishop, K. J. M. Microfluidic mixing of nonpolar liquids by contact charge electrophoresis. *Lab Chip* **2014**, *14*, 4230−4236.

(20) Dou, Y.; Cartier, C. A.; Fei, W.; Pandey, S.; Razavi, S.; Kretzschmar, I.; Bishop, K. J. M. Directed motion of metallodielectric particles by contact charge electrophoresis. *Langmuir* **2016**, *32*, 13167−13173.

(21) Zhang, Y.; Liu, Y.; Wang, X.; Shen, Y.; Ji, R.; Cai, B. Investigation of the charging characteristics of micrometer sized droplets based on parallel plate capacitor model. *Langmuir* **2013**, *29*, 1676−1682.

(22) Jung, Y. M.; Oh, H. C.; Kang, I. S. Electrical charging of a conducting water droplet in a dielectric fluid on the electrode surface. *J. Colloid Interface Sci.* **2008**, *322*, 617−623.

(23) Elton, E. S.; Rosenberg, E. R.; Ristenpart, W. D. Crater formation on electrodes during charge transfer with aqueous droplets or solid particles. *Phys. Rev. Lett.* **2017**, *119*, 094502.

(24) Tobazéon, R. Electrohydrodynamic behaviour of single spherical or cylindrical conducting particles in an insulating liquid subjected to a uniform DC field. *J. Phys. D: Appl. Phys.* **1996**, *29*, 2595−2608.

(25) Elton, E. S.; Tibrewala, Y.; Rosenberg, E. R.; Hamlin, B. S.; Ristenpart, W. D. Measurement of charge transfer to aqueous droplets in high voltage electric fields. *Langmuir* **2017**, *33*, 13945−13954.

(26) Pohl, H. A. *Dielectrophoresis*; Cambridge University Press: 1978.

(27) de la Mora, J. F. The fluid dynamics of Taylor cones. *Annu. Rev. Fluid Mech.* **2007**, *39*, 217−243.

(28) Hamlin, B. S.; Ristenpart, W. D. Transient reduction of the drag coefficient of charged droplets via the convective reversal of stagnant caps. *Phys. Fluids* **2012**, *24*, 012101.

(29) Birlasekaran, S.; Darveniza, M. Microdischarges from particles in transformer oil. *IEEE Trans. Electr. Insul.* **1976**, *EI-11*, 162−163.

(30) Drews, A. M.; Cartier, C. A.; Bishop, K. J. M. Contact charge electrophoresis: Experiment and theory. *Langmuir* **2015**, *31*, 3808−3814.

(31) Drews, A. M.; Kowalik, M.; Bishop, K. J. M. Charge and force on a conductive sphere between two parallel electrodes: A Stokesian dynamics approach. *J. Appl. Phys.* **2014**, *116*, 074903.

(32) Hadamard, J. S. Mouvement permanent lent d'une sphere liquide et visqueuse dans un liquide visqueux. *C. R. Acad. Sci.* **1911**, *152*, 1735−1743.

(33) Rybczynski, W. Über die fortschreitende bewegung einer flssigen kugel in einem zhen medium. *Bull. Acad. Sci. Cracovi, A* **1911**, 40−46.

(34) Yang, S. H.; Im, D. J. Electrostatic origins of the positive and negative charging difference in the contact charge electrophoresis of a water droplet. *Langmuir* **2017**, *33*, 13740−13748.

(35) Kuchmizhak, A.; Pavlov, D.; Vitrik, O.; Kulchin, Y. Laser ablative fabrication of nanocrowns and nanojets on the Cu supported film surface using femtosecond laser pulses. *Appl. Surf. Sci.* **2015**, *357*, 2378−2384.

DOI: 10.1021/acs.langmuir.8b01234
Langmuir 2018, 34, 7284−7293

(36) Koch, J.; Korte, F.; Bauer, T.; Fallnich, C.; Ostendorf, A.; Chichkov, B. Nanotexturing of gold films by femtosecond laser-induced melt dynamics. *Appl. Phys. A: Mater. Sci. Process.* **2005**, *81*, 325−328.
(37) Moening, J. P.; Georgiev, D. G.; Lawrence, J. G. Focused ion beam and electron microscopy characterization of nanosharp tips and microbumps on silicon and metal thin films formed via localized single-pulse laser irradiation. *J. Appl. Phys.* **2011**, *109*, 014304.
(38) Kuznetsov, A. I.; Unger, C.; Koch, J.; Chichkov, B. Laser-induced jet formation and droplet ejection from thin metal films. *Appl. Phys. A: Mater. Sci. Process.* **2012**, *106*, 479−487.
(39) Kuznetsov, A. I.; Koch, J.; Chichkov, B. N. Nanostructuring of thin gold films by femtosecond lasers. *Appl. Phys. A: Mater. Sci. Process.* **2009**, *94*, 221−230.
(40) Ivanov, D. S.; Lin, Z.; Rethfeld, B.; O'Connor, G. M.; Glynn, T. J.; Zhigilei, L. V. Nanocrystalline structure of nanobump generated by localized photoexcitation of metal film. *J. Appl. Phys.* **2010**, *107*, 013519.
(41) Meshcheryakov, Y. P.; Bulgakova, N. M. Thermoelastic modeling of microbump and nanojet formation on nanosize gold films under femtosecond laser irradiation. *Appl. Phys. A: Mater. Sci. Process.* **2006**, *82*, 363−368.
(42) Meshcheryakov, Y. P.; Shugaev, M. V.; Mattle, T.; Lippert, T.; Bulgakova, N. M. Role of thermal stresses on pulsed laser irradiation of thin films under conditions of microbump formation and non-vaporization forward transfer. *Appl. Phys. A: Mater. Sci. Process.* **2013**, *113*, 521−529.
(43) Serway, R. A., Ed.; *Physics for Scientists and Engineers*, 3rd ed.; Saunders College Publishing: 1990.
(44) Massala, G.; Lesaint, O. A comparison of negative and positive streamers in mineral oil at large gaps. *J. Phys. D: Appl. Phys.* **2001**, *34*, 1525−1532.
(45) Bruggeman, P.; Leys, C. Non-thermal plasmas in and in contact with liquids. *J. Phys. D: Appl. Phys.* **2009**, *42*, 053001.
(46) Bruggeman, P.; Guns, P.; Degroote, J.; Vierendeels, J.; Leys, C. Influence of the water surface on the glow-to-spark transition in a metal-pin-to-water electrode system. *Plasma Sources Sci. Technol.* **2008**, *17*, 045014.
(47) Sugimoto, T.; Asano, K.; Higashiyama, Y. Negative corona discharge at a tip of water cone deformed under DC field. *J. Electrost.* **2001**, *53*, 25−38.
(48) Lukes, P.; Clupek, M.; Babicky, V. Discharge filamentary patterns produced by pulsed corona discharge at the interface between a water surface and air. *IEEE Trans. Plasma Sci.* **2011**, *39*, 2644−2645.
(49) Miller, A. H.; Shelden, C. E.; Atkinson, W. R. Spectral study of the luminosity produced during coalescence of oppositely charged falling water drops. *Phys. Fluids* **1965**, *8*, 1921−1928.
(50) Sartor, J. D.; Atkinson, W. R. Charge transfer between raindrops. *Science* **1967**, *157*, 1267−1269.
(51) Mugele, F.; Baret, J. C. Electrowetting: from basics to applications. *J. Phys.: Condens. Matter* **2005**, *17*, R705.
(52) Calvert, P. Inkjet printing for materials and devices. *Chem. Mater.* **2001**, *13*, 3299−3305.
(53) Zolfaghari, R.; Fakhru'l-Razi, A.; Abdullah, L. C.; Elnashaie, S. S. E. H.; Pendashteh, A. Demulsification techniques of water-in-oil and oil-in-water emulsions in petroleum industry. *Sep. Purif. Technol.* **2016**, *170*, 377−407.
(54) Sugioka, K.; Cheng, Y. Femtosecond laser three-dimensional micro- and nanofabrication. *Appl. Phys. Rev.* **2014**, *1*, 041303.

DOI: 10.1021/acs.langmuir.8b01234
Langmuir 2018, 34, 7284−7293